CMS Physics Analysis Summary

Contact: cms-pag-conveners-bphysics@cern.ch 2024/04/30

Observation of a family of all-charm tetraquark candidates at the LHC

The CMS Collaboration

Abstract

Three structures, $X(6600)$, $X(6900)$, and $X(7100)$, have been reported in the $J/\psi J/\psi$ channel. These are prime candidates for all-charm tetraquarks. We extend our earlier study of these structures in proton-proton collisions using the CMS detector at the LHC, with 3.6 times more $J/\psi J/\psi$ pairs (315 fb^{-1} of total integrated luminosity). The statistical uncertainties on the masses and widths are reduced by about a factor of three, and the systematic uncertainties are also substantially reduced. For the first time all three structures are established with a significance well above five standard deviations (5σ). Good descriptions of the $J/\psi J/\psi$ spectrum were based on quantum interference among structures, which is now validated with significances of more than 5σ relative to the fit with no interference—implying all structures have the same J^{PC} quantum numbers, and suggests a family of states.

The proliferation of ostensibly "elementary" particles motivated Gell-Mann [1] and Zweig [2] to independently propose in 1964 that strongly interacting particles (hadrons) were composed of pairs ($q\overline{q}$ mesons), or triplets (qqq baryons), of quarks (q). Quarks, skeptically greeted as mathematical constructs, were accepted as physical entities by the mid-1970's—due significantly to the 1974 discovery of the charm (c) quark in the form of the J/ψ ($c\overline{c}$) meson around 3100 MeV [3, 4].

Gell-Mann and Zweig also noted in passing that the symmetry relations which underpinned their model also allowed tetra- and penta-quark systems. The possibility of "exotic" (neither $q\overline{q}$ nor qqq) hadrons was entertained for decades, but little was resolved. A primary difficulty was that in the light-quark (u, d, s) sector, excited hadrons have large natural widths, and exotic and standard hadrons overlap and mix, making unambiguous categorization problematic. By the close of the 20th century, it appeared that exotics may exist, but with no clear exemplars [5].

The turning point came in 2003 with the discovery of the $X(3872)$ meson in the $J/\psi\pi^+\pi^-$ channel [6]. This state appeared superficially to be an excited $c\overline{c}$ state, but its mass did not match expectations. Having a mass close to the $D^0\overline{D}^{*0}$ threshold, it was suggested that the $X(3872)$ meson was a weakly bound D^0-$\overline{D}^{*0}$ ($c\overline{u}$-$u\overline{c}$) "molecule" [7]. Many other heavy exotics were subsequently found [8, 9], including the manifestly exotic $Z(3930)^+ \to J/\psi\pi^+$ (i.e. $c\overline{d}$-$u\overline{c}$) [10, 11].

The key to establishing exotic hadrons was experimental access to the more tractable exotics containing heavy (c, b) quarks. Despite this seminal advance, controversies persist as to the internal structure of exotics. A variety of models have been proposed for the charmonium-like mesons: weakly-bound meson-meson molecules, hadro-charmonium (compact $c\overline{c}$ core embedded in an $q\overline{q}$ cloud), hybrids ($c\overline{c}$ core+valence gluon), or tightly bound system of four quarks (possibly structureless, or as a qq-$\overline{q}\overline{q}$ diquark system) [8]. It has also been argued that some exotics may arise from dynamical artifacts of production thresholds: threshold cusps, coupled-channel interactions, triangle singularities, or Pomeron exchange [8]. Just as having a heavy-quark component was key to establishing exotics, systems composed *entirely* of heavy quarks promise deeper insights and greater clarity.

This leap forward came with the discovery of the tetracharm candidates, $X(6600)$, $X(6900)$, and $X(7100)$—all seen in the $J/\psi J/\psi$ ($J/\psi \to \mu^+\mu^-$) channel. The $X(6600)$ was claimed by the CMS Collaboration with a local statistical significance of almost eight standard deviations (8σ) [12]; and although not asserted by them, the ATLAS and LHCb Collaborations saw structure [13, 14] that appears compatible. The $X(6900)$ structure—-the first discovered in 2020 by LHCb [13]—has been observed by all experiments with global significances above 5σ [12–14]. The $X(7100)$ evidence is weaker, 4.7σ locally (3.4σ globally) according to CMS. LHCb saw a hint of structure around 7.2 GeV, but neglected it because of its low significance [13]. ATLAS saw possible structure, according to one model of their $J/\psi\psi(2S)$ mass spectrum, around 7.2 GeV with a local significance of 3.0σ [14].

Despite these achievements, critical issues remain. The $X(7100)$ structure needs to be firmly established. All experiments preferred fit models utilizing quantum interference, but the models were incongruent and the interference was not statistically conclusive. In addition, all experiments reported an unexplained excess of J/ψ pairs just above the threshold.

However, the paramount question is whether these structures are indeed tetraquarks, and if so, of what sort. The configuration of four-quark systems potentially spans a broad dynamical continuum, but they are usually discussed in terms of idealized variants (see Ref. [8] and references therein).

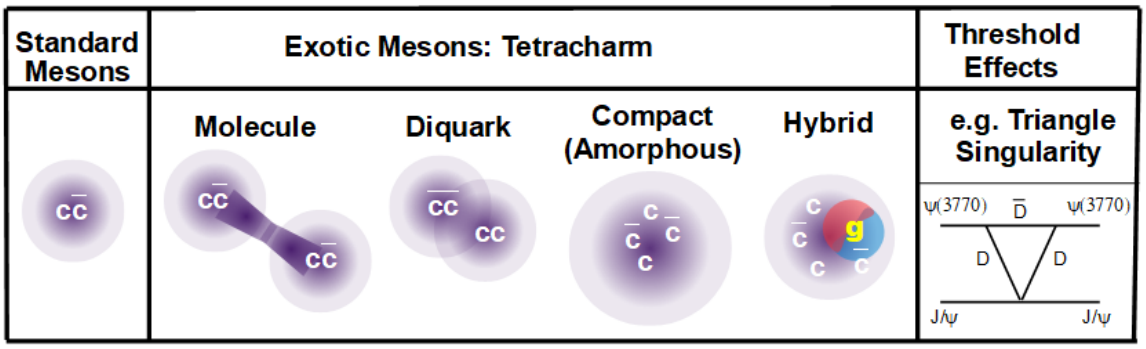

Figure 1: Idealized models of potential quark configurations for all-charm mesons. Far left: a conventional charmonium state, which is not a viable option for the very massive J/ψJ/ψ states. Center: various possibilities for tetraquarks—weakly bound molecule, cc-$\bar{c}\bar{c}$ diquark, and a compact tetraquark with amorphous substructure, and hybrid state of cc$\bar{c}\bar{c}$ plus valence gluon (g). Far right: one example of the class of non-resonant threshold effects, a triangle singularity, where, in this case, the scattering of J/ψ and $\psi(3770)$ mesons in production is enhanced through a triangular loop exchanging D mesons (the $\psi(3770)$ is an excited state of the J/ψ), and this could potentially lead to a peak-like structure in the J/ψJ/ψ mass around 6900 MeV [15].

The quarks may form a weakly bound meson-meson (c$\bar{c}$-c$\bar{c}$) "molecule," as a pair of "di-quarks" (cc-$\bar{c}\bar{c}$), an amorphous system with no substructure, or a hybrid where there is also a valence gluon [16] (Fig. 1). Two (anti)quarks in hadrons are believed to be weakly attracted to each other, such that they form a quasi-particle, a diquark [1]. Diquarks have been applied extensively, especially to model baryons, but the evidence has not been unambiguous [17]. Alternatively, some contend that the J/ψJ/ψ structures may actually be artifacts of dynamical effects of dicharmonia production thresholds [8]. Having three structures offers unique opportunities to address these questions.

In this note, we extend our previous results on the J/ψJ/ψ structures with 3.6 times more J/ψJ/ψ pairs from data collected through 2024, but still following, with minor variations, the same methods and models of Ref. [12].

The CMS detector and data selection

The CMS apparatus [18] is a large general purpose detector at CERN's Large Hadron Collider (LHC), with excellent capabilities for both high transverse momentum (p_T) physics (e.g. W, Z, and Higgs bosons) and lower p_T topics like heavy-quark hadron spectroscopy. Its main component is a superconducting solenoid with an internal diameter of 6 meters, capable of generating a magnetic field of 3.8 T. Inside the solenoid volume, there are a silicon pixel and strip tracker, a lead tungstate crystal electromagnetic calorimeter, and a brass and scintillator hadron calorimeter, each composed of a barrel and two end-cap sections. Muons ($\mu^{\pm}$) are identified using gas-ionization chambers, which are embedded in the steel flux-return yoke outside the solenoid.

Our previous analysis used 135 fb^{-1} of pp collisions from Run 2 (2016–18) at a center-of-mass energy ($\sqrt{s}$) of 13 TeV [12]. Here we add 180 fb^{-1} from Run 3 (2022–24) at $\sqrt{s} = 13.6$ TeV. Collisions of interest are recorded using a two-tiered trigger system [19]. The first level (L1) uses information from the calorimeters and muon detectors to select events, it is composed of custom hardware processors. The second level, referred as the high-level trigger (HLT), comprises a cluster of commercial processors running a faster version of the full event reconstruction software, resulting in an event rate reduction to a few kHz for recording.

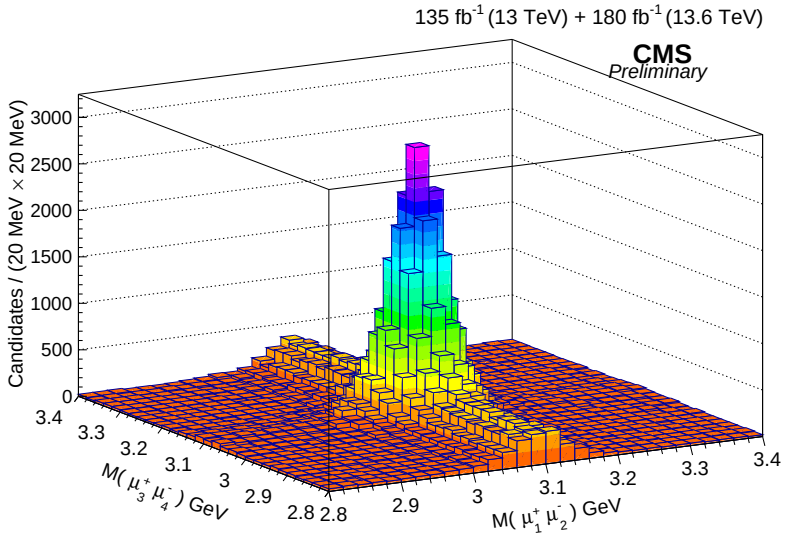

Figure 2: The two dimensional distribution of the double-dimuon masses for the final selection of J/ψJ/ψ events in the 6–15 GeV four-muon mass range for the Run 2+3 data. The two $\mu^+\mu^-$ pairs are ordered by their total transverse momentum (p_T).

The specific trigger selection relevant to this analysis varied somewhat over time, and the details may be found in Methods. In essence, the L1 selection required two or three muons, and in 2017–18 a minimum muon p_{T} as low as 3 GeV. The HLT required an oppositely charged dimuon to be within a dimuon mass window well covering the range near J/ψ mass, vertex consistency, and some versions also required two muons to have p_{T}'s above 3–4 GeV.

For the final offline event selection, we adhere to the original Run 2 criteria [12] for both the Run 2 and 3 datasets. The basic criteria are: there must be at least four muons with each having $p_{\mathrm{T}} > 2$ GeV; oppositely-charged pairs within three standard deviations (3σ) of the known J/ψ mass, a common vertex, and $p_{\mathrm{T}} > 3.5$ GeV; and a mass-constrained vertex fit applied to oppositely-charged muon pairs with their mass constrained to the known J/ψ mass.

From the final selection, we obtain $12\,622 \pm 165$ J/ψJ/ψ signal pairs in the 6–15 GeV J/ψJ/ψ mass range for Run 2 sample, and $31\,802 \pm 476$ signal events for Run 3 data. (Throughout this note, a single uncertainty is statistical only, dual uncertainties are statistical followed by systematic.) The Run 3 yield exceeds that of Run 2 by over 250%, despite its integrated luminosity being merely four-thirds of that in Run 2, by virtue of an enhanced trigger efficiency. A two-dimensional plot of the J/ψ vs. J/ψ candidate masses for the sample in the 6–15 GeV J/ψJ/ψ mass range is shown in Fig. 2. The J/ψJ/ψ mass distribution for candidates below 9 GeV is shown in Fig. 3—complex structures appear.

The J/ψJ/ψ mass spectrum and signal structures

The J/ψJ/ψ mass distribution from threshold to 15 GeV is fit using the unbinned extended likelihood method. The X signals are modeled by relativistic S-wave Breit–Wigner (BW) functions [20, 21], and for convenience, the BW functions for the $\mathrm{X}(6600)$, $\mathrm{X}(6900)$, and $\mathrm{X}(7100)$ structures are sequentially labeled as BW_1, BW_2, and BW_3. These functions are convolved with detector mass-resolution functions, derived from detector simulation, and are constructed by a sum of two Gaussian functions with identical mean values. The detector mass resolution varies from about 10 MeV at a mass of 6500 MeV to 18 MeV at 7300 MeV.

The background model has several components. At the high instantaneous luminosities of the

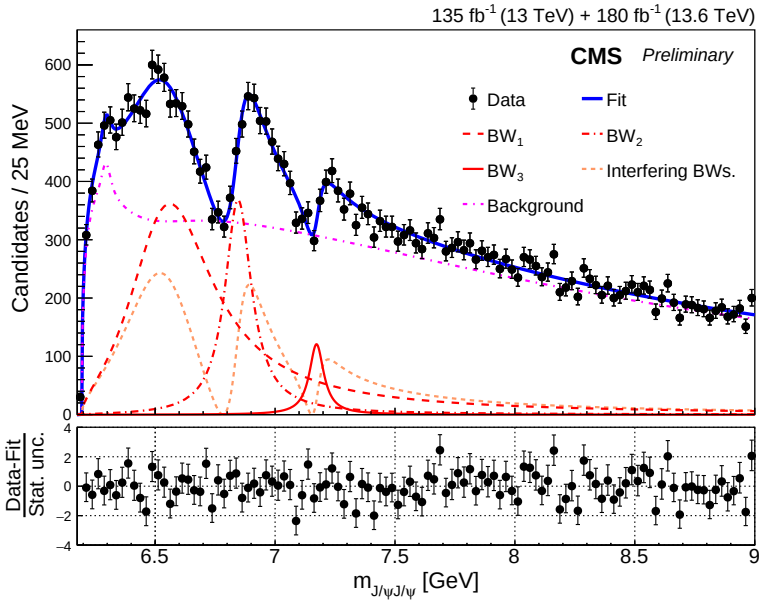

Figure 3: The selected J/ψJ/ψ invariant-mass spectrum up to 9 GeV. The data is fit (up to 15 GeV, see text) with the 3-way interference model, consisting of three signal functions (BW_1, BW_2, and BW_3), a background threshold BW_0, and background components (NRSPS, DPS, combinatoric, and $X(6900)\to J/\psi\psi(2S)$ feeddown). The cumulative squared amplitude of the interfering signals is also shown. The lower panel shows the deviations of the data points from the fitted curve in standard deviations.

LHC, double-parton scattering (DPS) will occur, where two hard parton-parton interactions within the same pp collision can produce two independent J/ψ mesons. This is in contrast to the normal nonresonant single-parton scattering (NRSPS) in an individual proton collision. NRSPS tends to dominate at low J/ψJ/ψ masses. The parameterized shape for DPS is derived from the event-mixing of data, while the NRSPS parameters are fixed from simulation, except one parameter for an exponential component of the parameterization, floating in the J/ψJ/ψ mass fit of the data.

Combinatorial backgrounds arise when one or more muon candidates are not from a J/ψ meson: random muon parings, hadrons misidentified as a muon, or misreconstructed muons. The shape of the combinatorial background is obtained from off-peak data via the so-called "Ninetile" method [22], and verified by sPlot [23]. The yield of the combinatorial background is estimated from a background subtraction method using a two-dimensional $m(J/\psi_1)$ v. $m(J/\psi_2)$ fit. The mean and uncertainty of this yield are used as a Gaussian constraint of the combinatorial component in the full J/ψJ/ψ mass likelihood fit. The uncertainties are around 7% and the fitted result stays within the uncertainties.

Another background is feeddown from higher-mass states, such as $X\to J/\psi\psi(2S)$, where $\psi(2S)$ can, for example, decay to $J/\psi\pi^0\pi^0$ and the $\pi^0\pi^0$ are lost to the reconstruction. In our previous study, this was treated as a systematic uncertainty due to its speculative nature. Since then, ATLAS has reported a significant near-threshold excess in the $J/\psi\psi(2S)$ channel [14], and CMS identified $J/\psi\psi(2S)$ structure consistent with $X(6900)$ decays, and evidence for a $X(7100)\to J/\psi\psi(2S)$ signal [24]. Feeddown from this source is now part of our baseline model. We generated the feeddown processes from double-charmonium resonances [25] using the PYTHIA generator [26–31]. A state with a mass of 6847 MeV is generated with a width of 191 MeV [12], which decays into the $J/\psi\psi(2S)$, and $\psi(2S)\to J/\psi + anything$. These events are

processed through the full CMS detector simulation. A parameterization of this shape, with floating normalization, is included in our fit.

Aside from the above backgrounds, the three LHC experiments reported a near-threshold excess of candidates above background [12–14], which all were reluctant to interpret. While this might be due to a resonance, there are other possibilities such as coupled-channel interactions [32], triangular singularities [33], Pomeron exchange [34], unknown feeddown, or just an inadequate NRSPS model. Because of this uncertainty, we relegate this excess to our background model. A BW function, BW_0, serves as a good *ad hoc* description of this excess.

To fit the J/ψJ/ψ spectrum, we adopt our previous models [12]. Our baseline fit consists of three BW functions plus NRSPS, DPS, combinatoric, a threshold background BW_0 and feeddown backgrounds. We employ a "three-way" Breit–Wigner interference model for the three BW_j signals. Interference is introduced through a term proportional to $|r_1 \times e^{i\phi_1} \times \mathrm{BW}_1 + \mathrm{BW}_2 + r_3 \times e^{i\phi_3} \times \mathrm{BW}_3|^2$, where r_j and ϕ_j are the relative magnitude and phase angle of BW_j with respect to BW_2. The threshold background, BW_0, is treated as a non-interfering BW function, and is implemented with a term proportional to $|\mathrm{BW}_0|^2 \otimes R(M_0)$, where $R(M_0)$ is the resolution at mass M_0. For reference, we also consider our "no-interference" model [12] in Supplemental Material, where none of the fit components interfere, i.e. all BW terms are proportional to $|\mathrm{BW}_j|^2 \otimes R(M_j)$, for $j = 0, 1, 2$, and 3.

The result of the interference fit is shown in Fig. 3. The fit extends up to a mass of 15 GeV in order to better determine the DPS normalization, but to clearly show the signal region, we display the spectrum only up to 9 GeV (full fit range is provided in Supplementary Material). The figure shows the decomposition into the various components, as well as the total squared-amplitude of the signal BW's. The hump of background component arises from the feeddown contribution, which nearly dominates at the threshold, and also a BW_0 contribution at a somewhat higher mass, which indicates the presence of some additional source of the near-threshold events.

The fit quality is assessed by the χ^2 per-degree-of-freedom of the fit (with the bin size of Fig. 3), which is 1.04 (346/334). However, the signal region is only a small portion of the full fit and any localized χ^2 discrepancies there will be heavily diluted by the broad high-mass continuum. To address this, we also calculate the χ^2 per-degree-of-freedom for only the range of 6.2–7.8 GeV. Over this restricted range, our quality metric is 1.15 (52/45). This is in stark contrast to the value of 3.09 (145/47) which we obtain from the no-interference fit, underscoring the important introduction of interference. Furthermore, in the interference model, the significance of interference is 9.9σ for the two dips.

The results of the J/ψJ/ψ interference fit are listed in Table 1, along with a copy of the previous Run 2 values [12]. The fit of the Run 2+3 data significantly improves our precision, with the statistical uncertainties on the triplet parameters improving, in most cases, by about a factor of three.

The local significances of the structures in the Run 2+3 interference fit, computed from the log-likelihood differences between the complete fit and the fit with the respective BW_j component removed, are 15.2σ, 16.7σ, and 7.7σ, for increasing X mass. The $\mathrm{X}(7100)$ structure now exceeds 5σ in a single experiment for the first time, firmly establishing a collection of three structures. The impact of systematic uncertainties on the local significance of the BW_3 structure was checked by using discrete sets of individual alternative hypotheses and recomputing the significance—there was no appreciable reduction.

The spectra from all three LHC experiments preferred models employing interference [12–14],

Table 1: Fit results of the J/ψJ/ψ mass spectra for various data sets with interference in MeV (uncertainties are statistical followed by systematic). The "Run 2" result is a copy of Ref. [12] for comparison.

		BW_1	BW_2	BW_3
Interference	m (MeV)	$6593\ ^{+15}_{-14} \pm 25$	$6847\ ^{+10}_{-10} \pm 15$	$7173\ ^{+9}_{-10} \pm 13$
(Run 2+Run 3)	Γ (MeV)	$446\ ^{+66}_{-54} \pm 87$	$135\ ^{+16}_{-14} \pm 14$	$73\ ^{+18}_{-15} \pm 10$
Interference	m (MeV)	$6638\ ^{+43+16}_{-38-31}$	$6847\ ^{+44+48}_{-28-20}$	$7134\ ^{+48+41}_{-25-15}$
(Run 2 [12])	Γ (MeV)	$440\ ^{+230+110}_{-200-240}$	$191\ ^{+66+25}_{-49-17}$	$97\ ^{+40+29}_{-29-26}$

in some form, yet it was not statistically conclusive (i.e. not $> 5\sigma$) for any of them. To evaluate the significance of interference, we re-fit the data by selectively removing specific interference terms. We compared fits where only one pair of resonances interfere (e.g., BW_1-BW_2) to fits where all interference terms are included. The difference in log-likelihoods between the full interference fit and these reduced-interference fits are used to derive the significance of individual interference terms. The significance of the first interference dip around 6750 MeV is 9.7σ, while the second dip around 7150 MeV has a significance of 6.5σ.

Summary

We have extended our study of the J/ψJ/ψ mass spectrum with 3.6 times more J/ψJ/ψ pairs. The spectrum is well described by mutually interfering $X(6600)$, $X(6900)$, and $X(7100)$ structures. The statistical uncertainties on their masses and widths are reduced by a factor of three over our previous results [12]. For the first time, all three structures are established with a significance well above five standard deviations (5σ). Similarly, interference among the three structures is now statistically compelling. Interference implies that the structures have common J^{PC} quantum numbers—suggesting a family of states. Recently CMS reported an angular analysis of the X$\rightarrow$J/ψJ/ψ decay characteristics and found the J^{PC} quantum numbers of the X family is most likely 2^{++} [35].

References

[1] M. Gell-Mann, "A schematic model of baryons and mesons", *Phys. Lett.* **8** (1964) 214, doi:10.1016/S0031-9163(64)92001-3.

[2] G. Zweig, "An SU(3) model for strong interaction symmetry and its breaking", 1964. CERN-TH-401, doi:10.17181/CERN-TH-401.

[3] E598 Collaboration, "Experimental observation of a heavy particle J", *Phys. Rev. Lett.* **33** (1974) 1404, doi:10.1103/PhysRevLett.33.1404.

[4] SLAC-SP-017 Collaboration, "Discovery of a narrow resonance in e^+e^- annihilation", *Phys. Rev. Lett.* **33** (1974) 1406, doi:10.1103/PhysRevLett.33.1406.

[5] L. G. Landsberg, "The search for exotic hadrons", *Phys. Usp.* **42** (1999) 871, doi:10.1070/PU1999v042n09ABEH000579.

[6] Belle Collaboration, "Observation of a narrow charmonium-like state in exclusive $B^{\pm} \to K^{\pm}\pi^{+}\pi^{-}J/\psi$ decays", *Phys. Rev. Lett.* **91** (2003) 262001, doi:10.1103/PhysRevLett.91.262001, arXiv:hep-ex/0309032.

[7] F. E. Close and P. R. Page, "The D^{*0} anti-D^{0} threshold resonance", *Phys. Lett. B* **578** (2004) 119–123, doi:10.1016/j.physletb.2003.10.032, arXiv:hep-ph/0309253.

[8] H.-X. Chen et al., "An updated review of the new hadron states", *Rept. Prog. Phys.* **86** (2023), no. 2, 026201, doi:10.1088/1361-6633/aca3b6, arXiv:2204.02649.

[9] A. Ali, L. Maiani, and A. D. Polosa, "Multiquark Hadrons". Cambridge University Press, 2019. doi:10.1017/9781316761465, ISBN 978-1-316-76146-5, 978-1-107-17158-9, 978-1-316-77419-9.

[10] BESIII Collaboration, "Observation of a charged charmoniumlike structure in $e^{+}e^{-} \to \pi^{+}\pi^{-}J/\psi$ at $\sqrt{s}$ =4.26 GeV", *Phys. Rev. Lett.* **110** (2013) 252001, doi:10.1103/PhysRevLett.110.252001, arXiv:1303.5949.

[11] Belle Collaboration, "Study of $e^{+}e^{-} \to \pi^{+}\pi^{-}J/\psi$ and observation of a charged charmoniumlike state at Belle", *Phys. Rev. Lett.* **110** (2013) 252002, doi:10.1103/PhysRevLett.110.252002.

[12] CMS Collaboration, "Observation of new structure in the J/ψJ/ψ mass spectrum in proton-proton collisions at $\sqrt{s}$ = 13 TeV", *Phys. Rev. Lett.* (2024) arXiv:2306.07164.

[13] LHCb Collaboration, "Observation of structure in the J/ψ-pair mass spectrum", *Sci. Bull.* **65** (2020) 1983, doi:10.1016/j.scib.2020.08.032, arXiv:2006.16957.

[14] ATLAS Collaboration, "Observation of an excess of dicharmonium events in the four-muon final state with the ATLAS detector", *Phys. Rev. Lett.* **131** (2023), no. 15, 151902, doi:10.1103/PhysRevLett.131.151902, arXiv:2304.08962.

[15] Y. Lu, C. Chen, G.-y. Qin, and H.-Q. Zheng, "A discussion on the anomalous threshold enhancement of J/ψ–$\psi(3770)$ couplings and $X(6900)$ peak", *Chin. Phys. C* **48** (2024), no. 4, 041001, doi:10.1088/1674-1137/ad2361, arXiv:2312.10711.

[16] B.-D. Wan and C.-F. Qiao, "Gluonic tetracharm configuration of X(6900)", *Phys. Lett. B* **817** (2021) 136339, doi:10.1016/j.physletb.2021.136339, arXiv:2012.00454.

[17] M. Y. Barabanov et al., "Diquark correlations in hadron physics: Origin, impact and evidence", *Prog. Part. Nucl. Phys.* **116** (2021) 103835, doi:10.1016/j.ppnp.2020.103835, arXiv:2008.07630.

[18] CMS Collaboration, "The CMS Experiment at the CERN LHC", *JINST* **3** (2008) S08004, doi:10.1088/1748-0221/3/08/S08004.

[19] CMS Collaboration, "The CMS trigger system", *JINST* **12** (2017), no. 01, P01020, doi:10.1088/1748-0221/12/01/P01020, arXiv:1609.02366.

[20] Particle Data Group Collaboration, "Review of Particle Physics", *PTEP* **2020** (2020), no. 8, 083C01, doi:10.1093/ptep/ptaa104.

[21] A. R. Bohm and Y. Sato, "Relativistic resonances: Their masses, widths, lifetimes, superposition, and causal evolution", *Phys. Rev. D* **71** (2005) 085018, doi:10.1103/PhysRevD.71.085018, arXiv:hep-ph/0412106.

[22] CMD-3 Collaboration, "Study of the process $e^+e^- \to K_S^0 K_S^0 \pi^+\pi^-$ in the c.m. energy range 1.6–2.0 GeV with the CMD-3 detector", *Phys. Lett. B* **804** (2020) 135380, doi:10.1016/j.physletb.2020.135380, arXiv:1912.05751.

[23] M. Pivk and F. Le Diberder, "sPlot: A statistical tool to unfold data distributions", *Nuclear Instruments and Methods in Physics Research Section A: Accelerators, Spectrometers, Detectors and Associated Equipment* **555** (2005), no. 12, 356369, doi:10.1016/j.nima.2005.08.106, arXiv:physics/0402083.

[24] CMS Collaboration, "Observation of $\mathrm{X}(6900)$ and evidence of $\mathrm{X}(7100)$ in the $\mathrm{J}/\psi\psi(2S) \to \mu^+\mu^-\mu^+\mu^-$ mass spectrum in pp collisions at CMS", *CMS PAS-BPH-22-004* (2025).

[25] J.-Z. Wang, X. Liu, and T. Matsuki, "Fully-heavy structures in the invariant mass spectrum of $\mathrm{J}/\psi\psi(3686)$, $\mathrm{J}/\psi\psi(3770)$, $\psi(3686)\psi(3686)$, and $\mathrm{J}/\psi\mathrm{Y}(1\mathrm{S})$ at hadron colliders", *Phys. Lett. B* **816** (2021) 136209, doi:10.1016/j.physletb.2021.136209, arXiv:2012.03281.

[26] T. Sjöstrand, S. Mrenna, and P. Skands, "A brief introduction to PYTHIA 8.1", *Computer Physics Communications* **178** (2008), no. 11, 852–867, doi:10.1016/j.cpc.2008.01.036.

[27] H. Jung et al., "The CCFM monte carlo generator CASCADE Version 2.2.03", *The European Physical Journal C* **70** (2010), no. 4, 1237–1249, doi:10.1140/epjc/s10052-010-1507-z.

[28] H.-S. Shao, "HELAC-Onia: An automatic matrix element generator for heavy quarkonium physics", *Computer Physics Communications* **184** (2013), no. 11, 2562–2570, doi:10.1016/j.cpc.2013.05.023.

[29] J.-P. Lansberg and H.-S. Shao, "J/ψ-pair production at large momenta: Indications for double parton scatterings and large α_s^5 contributions", *Physics Letters B* **751** (2015) 479–486, doi:10.1016/j.physletb.2015.10.083.

[30] J.-P. Lansberg and H.-S. Shao, "Production of $J/\psi + \eta_c$ versus $J/\psi + J/\psi$ at the LHC: Importance of real α_s^5 corrections", *Physical Review Letters* **111** (2013), no. 12, doi:10.1103/physrevlett.111.122001.

[31] H.-S. Shao, "HELAC-Onia 2.0: an upgraded matrix-element and event generator for heavy quarkonium physics", *Comput. Phys. Commun.* **198** (2016) 238–259, doi:10.1016/j.cpc.2015.09.011, arXiv:1507.03435.

[32] X.-K. Dong et al., "Coupled-Channel Interpretation of the LHCb Double- J/ψ Spectrum and Hints of a New State Near the $J/\psi J/\psi$ Threshold", *Phys. Rev. Lett.* **126** (2021), no. 13, 132001, doi:10.1103/PhysRevLett.126.132001, arXiv:2009.07795. Erratum: Phys. Rev. Lett. 127, 119901 (2021).

[33] F.-K. Guo, X.-H. Liu, and S. Sakai, "Threshold cusps and triangle singularities in hadronic reactions", *Prog. Part. Nucl. Phys.* **112** (2020) 103757, doi:10.1016/j.ppnp.2020.103757, arXiv:1912.07030.

[34] C. Gong et al., "Nature of X(6900) and its production mechanism at LHCb", *Phys. Lett. B* **824** (2022) 136794, doi:10.1016/j.physletb.2021.136794, arXiv:2011.11374.

[35] CMS Collaboration, "Spin and symmetry properties of all-charm tetraquarks", *CMS PAS-BPH-24-002* (2025).

[36] CMS Collaboration, "Performance of CMS muon reconstruction in pp collision events at $\sqrt{s} = 7$ TeV", *JINST* **7** (2012) P10002, doi:10.1088/1748-0221/7/10/P10002, arXiv:1206.4071.

[37] Y. Gao et al., "Spin determination of single-produced resonances at hadron colliders", doi:10.1103/PhysRevD.81.075022, arXiv:1001.3396.

[38] S. Bolognesi et al., "On the spin and parity of a single-produced resonance at the LHC", doi:10.1103/PhysRevD.86.095031, arXiv:1208.4018.

[39] I. Anderson et al., "Constraining anomalous HVV interactions at proton and lepton colliders", doi:10.1103/PhysRevD.89.035007, arXiv:1309.4819.

[40] A. V. Gritsan, R. Rontsch, M. Schulze, and M. Xiao, "Constraining anomalous *Higgs* boson couplings to the heavy flavor fermions using matrix element techniques", doi:10.1103/PhysRevD.94.055023, arXiv:1606.03107.

[41] A. V. Gritsan et al., "New features in the JHU generator framework: Constraining Higgs boson properties from on-shell and off-shell production", *Physical Review D* **102** (2020), no. 5, doi:10.1103/physrevd.102.056022, arXiv:2002.09888.

[42] GEANT4 Collaboration, "GEANT4–a simulation toolkit", *Nucl. Instrum. Meth. A* **506** (2003) 250–303, doi:10.1016/S0168-9002(03)01368-8.

Methods

Online Trigger. The detailed trigger conditions used for data collection are as follows:

- 2016 Run 2 data [36.3 fb^{-1}]: The L1 trigger required a minimum of three muon candidates. The HLT mandated that each muon's pseudorapidity satisfies $|\eta| < 2.5$, and a pair of muons with opposite charge and an invariant mass ranging from 2.95 to 3.25 GeV, a distance of closest approach between the two muons less than 0.5 cm, and a fit to a common vertex with a χ^2 probability greater than 0.5%.
- 2017–18 Run 2 data [98.6 fb^{-1}]: The L1 trigger required a minimum of three muons, with at least two having p_{T}>3 GeV and one of these having p_{T}>4.9 GeV, as well as at least one oppositely charged pair of muons with invariant mass below 9 GeV. The HLT criteria replicated those of 2016 with the added stipulation that the two muons with invariant mass between 2.95 and 3.25 GeV each must have $p_{\text{T}} > 3.5$ GeV.
- 2022–24 Run 3 data [180 fb^{-1}]: The L1 trigger had two paths, a three-muon trigger identical to the 2017–18 trigger, and a new two muon trigger. This analysis used the logical "OR" of the two. The corresponding HLT trigger demanded at least one pair of oppositely charged muons with a mass below 8.5 GeV. At least one muon of the pair is required to have $p_{\text{T}} > 4$ GeV, while the other must have $p_{\text{T}} > 3$ GeV.

Offline Selection. For the final event selection, we adhere to the original Run 2 criteria [12] for both the Run 2 and 3 datasets to make the new analysis a simple and direct extension of the Run 2 results. The detailed criteria are as follows.

There must be at least four muons satisfying the "soft muon identification" requirements [36], while each of them has $p_{\text{T}} > 2$ GeV and $|\eta| < 2.4$. Muon pairs of opposite charge are used to form J/ψ candidates, required to have $p_{\text{T}} > 3.5$ GeV and a fit probability greater than 0.5% when fitting to a vertex. In addition, a fit probability must be greater than 0.5% when combinations of four muons from two J/ψ are fit to a common vertex, while the probability must exceed 0.1% for the two constrained J/ψ candidates. A mass constrained vertex fit is applied to muon pairs with opposite charge, in which the muon pair's mass is constrained to the known J/ψ mass of 3.096 GeV, and the probability is required to be greater than 0.1%.

Multiple J/ψ candidates may be included in a single event. If both charge permutations of the same four muons have masses within 3 standard deviations (3σ) of the known J/ψ mass, we select the pairing that minimizes $(\triangle m_1/\sigma_{m_1})^2 + (\triangle m_2/\sigma_{m_2})^2$, where $\triangle m$ is the difference between the constructed dimuon mass and the J/ψ mass, and the σ_m is the calculated uncertainty of the reconstructed dimuon mass. All J/ψJ/ψ candidates are kept if they arise from more than four muons.

Simulation. Monte Carlo event generators are used to simulate both signal and background events. Signal samples were simulated by generating conventional $J^P = 0^+$ mesons of different masses with 1 MeV natural width, decaying to J/ψJ/ψ, they were produced via gluon-gluon collisions by the JHUGen generator (version 7.40) [37–41]. Samples of non-resonant single-parton (NRSPS) were produced using the PYTHIA generator [26–31], and included both direct production and feeddown processes producing J/ψ mesons. Feeddown processes from double-charmonium resonances [25] are generated using the PYTHIA generator. Generated events were processed through the full CMS detector simulation, which is based on the GEANT4 [42] simulation of particle interactions with materials.

Systematic uncertainties. Systematic uncertainties for masses and widths are evaluated by varying various aspects and inputs of the fitting procedures. The systematic uncertainty for a

Table 2: The dominant contributions to the systematic uncertainties, in MeV, for the triplet for our main fit.

Dominant sources	Δm_{BW_1}	$\Delta\Gamma_{\mathrm{BW}_1}$	Δm_{BW_2}	$\Delta\Gamma_{\mathrm{BW}_2}$	Δm_{BW_3}	$\Delta\Gamma_{\mathrm{BW}_3}$
Signal shape	25	52	2	11	3	5
NRSPS shape	3	7	<1	1	<1	5
DPS shape	<1	5	<1	<1	<1	1
Combinatorial bkg shape	<1	22	<1	2	<1	4
Feeddown	<1	1	<1	<1	<1	<1
Mass resolution	4	58	15	7	12	5
Efficiency	<1	4	<1	<1	<1	<1
Without BW_0	<1	29	2	3	2	1
Total uncertainty	25	87	15	14	13	10

given parameter is defined as the largest deviation from its nominal value observed when these factors are altered. The sources of systematic uncertainty include: different BW shapes, combinatorial background shape, detector mass resolution, NRSPS and DPS parameterizations, feeddown components ($\mathrm{X}(7100)\to\mathrm{J}/\psi\psi(2\mathrm{S})$), efficiency corrections, and the effects of BW_0. The principal systematic effects are summarized in Table 2. The total uncertainties are the sums of individual contributions in quadrature.

Supplemental material

J/ψJ/ψ spectrum over the full fit range

The J/ψJ/ψ spectrum and fit shown in Fig. 3 (main text) is truncated at 9 GeV in order to clearly display the X structure at the lower masses, but the fit extends up to a mass of 15 GeV. The J/ψJ/ψ invariant mass spectrum and fit for the full fit range is shown in Fig. 4 for the interference model.

Comparison of J/ψJ/ψ fit results including the no-interference model

For comparative purposes Table 3 collects various fits of the J/ψJ/ψ mass spectra. The results from the Run 2 interference fit [12] are reproduced in the first data column. Because the current analysis includes the feeddown contribution, which was only accounted for as a systematic in the published result, the second fit column shows an updated fit of the same Run 2 data with the feeddown component now included in the fit. The central mass and width parameters do not change much, but statistical errors systematically decrease.

The next column shows the baseline interference fit model using only Run 3 data; and then, for convenience, we reproduce the fit from the main body of the paper where the Run 2 and 3 data are combined. The final column shows the combined fit where the no-interference fit model from Ref. [12] is used: i.e. none of the BW functions interfere and they are simple additive contributions.

J/ψJ/ψ spectrum with the Run 3 data

As shown in Fig. 5, the comparison plot of J/ψJ/ψ spectrum for the separate Run 2 and Run 3 data also indicate the presence of structures in the Run 3 data only. The yield per unit luminos-

Table 3: Fit results of the J/ψJ/ψ mass spectra for various data sets in MeV (dual uncertainties are statistical followed by systematic, single uncertainties are statistical only). Our baseline fit is Run 2+Run 3 data with interference (reproduced from main text).

Parameter	Run 2 [12] [Interf.]	Run 2 (updated) [Interf.]	Run 3 [Interf.]	Run 2 + 3 [Interf.]	Run 2 + 3 [No-Interf.]
$m(\mathrm{BW}_1)$	$6638\ ^{+43+16}_{-38-31}$	6620 ± 30	6588 ± 19	$6593\ ^{+15}_{-14} \pm 25$	6540 ± 8
$\Gamma(\mathrm{BW}_1)$	$440\ ^{+230+110}_{-200-240}$	422 ± 154	454 ± 74	$446\ ^{+66}_{-54} \pm 87$	142 ± 19
$m(\mathrm{BW}_2)$	$6847\ ^{+44+48}_{-28-20}$	6856 ± 27	6849 ± 12	$6847\ ^{+10}_{-10} \pm 15$	6927 ± 6
$\Gamma(\mathrm{BW}_2)$	$191\ ^{+66+25}_{-49-17}$	176 ± 43	136 ± 18	$135\ ^{+16}_{-14} \pm 14$	97 ± 13
$m(\mathrm{BW}_3)$	$7134\ ^{+48+41}_{-25-15}$	7159 ± 28	7179 ± 10	$7173\ ^{+9}_{-10} \pm 13$	7247 ± 8
$\Gamma(\mathrm{BW}_3)$	$97\ ^{+40+29}_{-29-26}$	90 ± 26	67 ± 18	$73\ ^{+18}_{-15} \pm 10$	37 ± 24

ity increases from 93 events/ fb^{-1} in Run 2 to 177 events/ fb^{-1} in Run 3. And as computed from the log-likelihood differences, the local significances of the three structures and two dips are all above 5σ. The J/ψJ/ψ spectrum fit with only Run 3 data are as shown in Fig. 6. Additionally, the lower panel of Fig. 5 compares Run 2 with the combined Run 2+3.

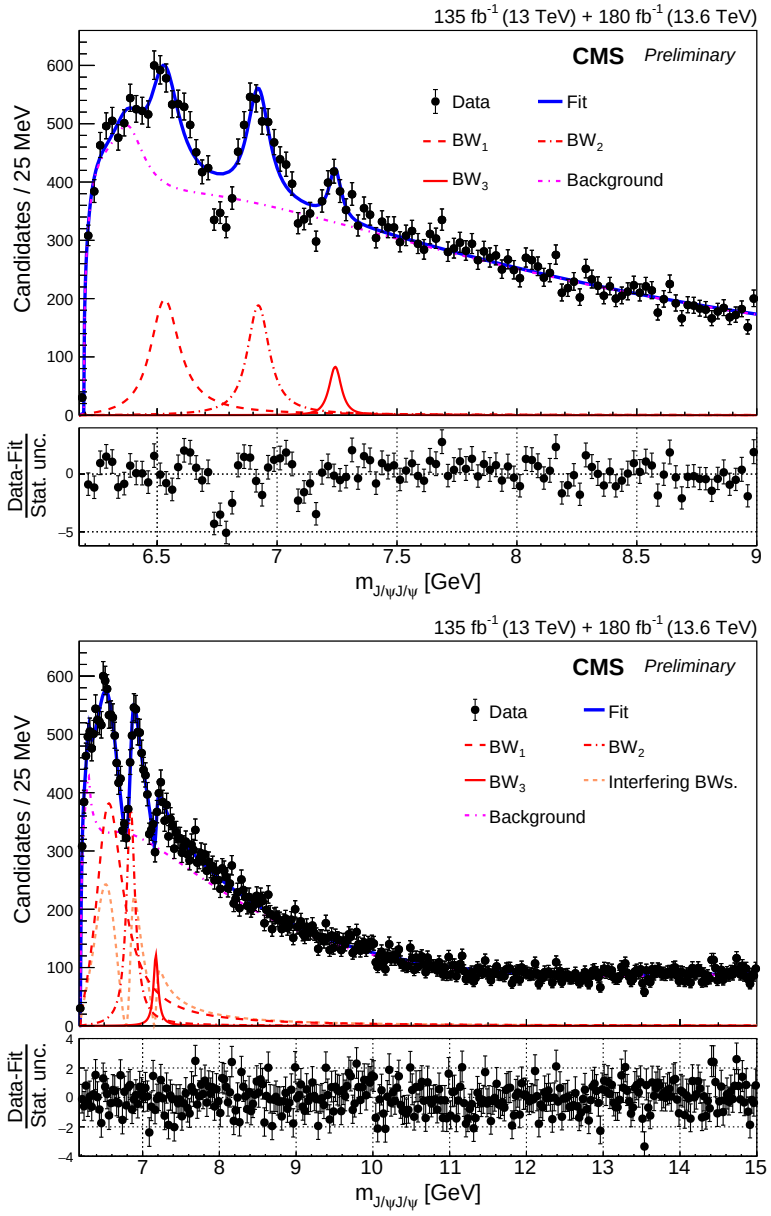

Figure 4: The J/ψJ/ψ invariant mass spectrum for the no-interference in the 6–9 GeV four-muon mass range (upper) and the interference fit for the full fit range (lower) (see text in the main paper for model details). The curve labeled "Interfering BWs" represents the total contribution from all interference amplitudes and their cross terms. The lower panels of the plots display the number of standard deviations (considering only statistical uncertainties) by which the binned data deviate from the fit.

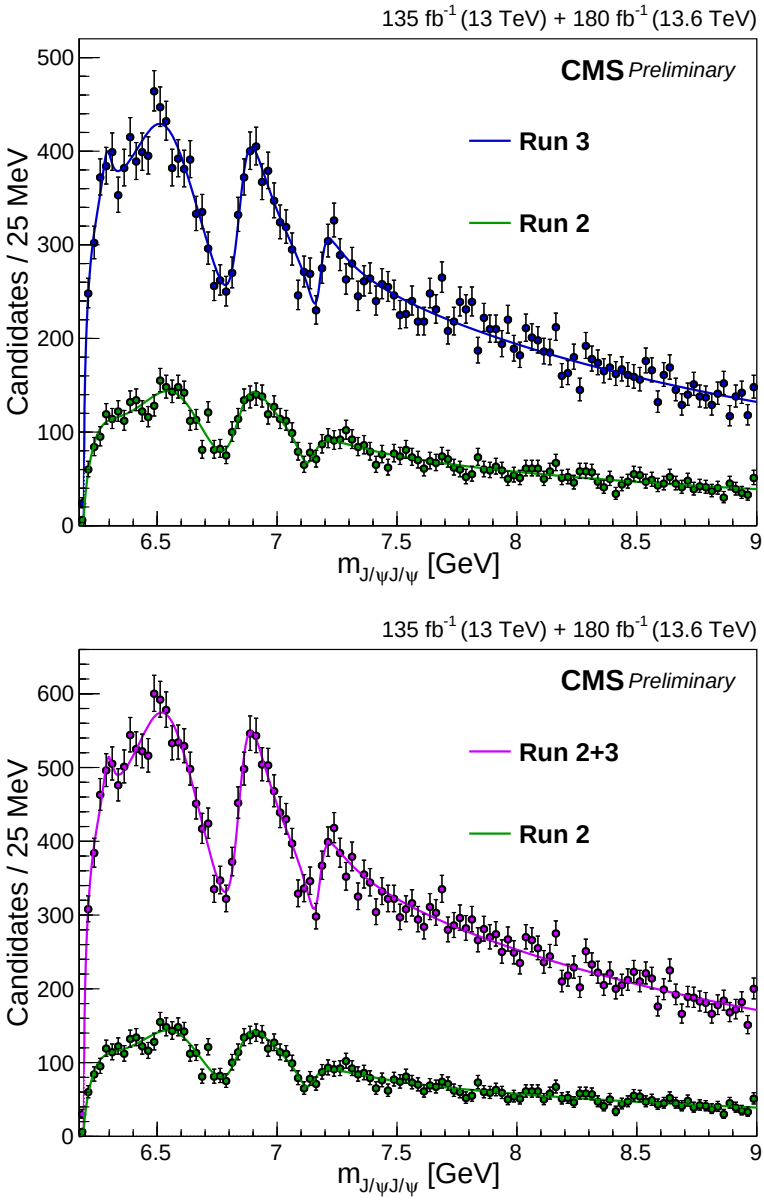

Figure 5: The J/ψJ/ψ invariant mass spectrum for the individual Run 2 and Run 3 datasets (upper), and for Run 2 compared with the combined Run 2+3 dataset (lower).

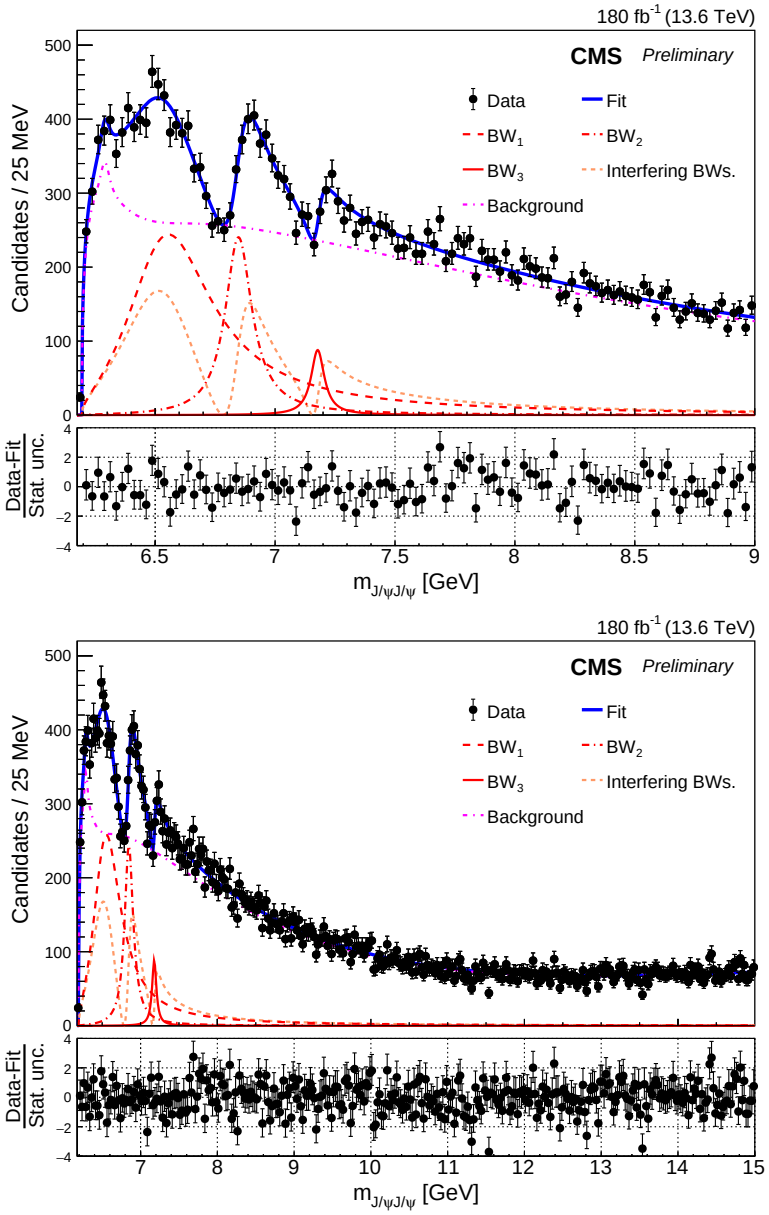

Figure 6: The J/ψJ/ψ invariant mass spectrum for the interference fit for the 6–9 GeV range (upper) and the full fit range (lower) with the Run 3 data. The curve labeled "Interfering BWs" represents the total contribution from all interference amplitudes and their cross terms. The lower panels of the plots display the number of standard deviations (considering only statistical uncertainties) by which the binned data deviate from the fit.